Mathematical and Computational Applications

MDPI

Article

Entropy Generation of Cu–Al_2O_3/Water Flow with Convective Boundary Conditions through a Porous Stretching Sheet with Slip Effect, Joule Heating and Chemical Reaction

Maria Immaculate Joyce [1], Jagan Kandasamy [1,*] and Sivasankaran Sivanandam [2]

[1] Department of Mathematics, School of Engineering, Presidency University, Bangalore 560064, India
[2] Mathematical Modelling and Applied Computation Research Group, Department of Mathematics, King Abdulaziz University, Jeddah 21589, Saudi Arabia
* Correspondence: kjaganppmaths@gmail.com

Abstract: Currently, the efficiency of heat exchange is not only determined by enhancements in the rate of heat transfer but also by economic and accompanying considerations. Responding to this demand, many scientists have been involved in improving heat transfer performance, which is referred to as heat transfer enhancement, augmentation, or intensification. This study deals with the influence on hybrid Cu–Al_2CO_3/water nanofluidic flows on a porous stretched sheet of velocity slip, convective boundary conditions, Joule heating, and chemical reactions using an adapted Tiwari–Das model. Nonlinear fundamental equations such as continuity, momentum, energy, and concentration are transmuted into a non-dimensional ordinary nonlinear differential equation by similarity transformations. Numerical calculations are performed using HAM and the outcomes are traced on graphs such as velocity, temperature, and concentration. Temperature and concentration profiles are elevated as porosity is increased, whereas velocity is decreased. The Biot number increases the temperature profile. The rate of entropy is enhanced as the Brinkman number is raised. A decrease in the velocity is seen as the slip increases.

Keywords: hybrid nanofluid; convective; Joule heating; porosity; stretching sheet; chemical reaction

Citation: Joyce, M.I.; Kandasamy, J.; Sivanandam, S. Entropy Generation of Cu–Al_2O_3/Water Flow with Convective Boundary Conditions through a Porous Stretching Sheet with Slip Effect, Joule Heating and Chemical Reaction. *Math. Comput. Appl.* **2023**, *28*, 18. https://doi.org/10.3390/mca28010018

Academic Editor: Zhuojia Fu

Received: 15 November 2022
Revised: 23 January 2023
Accepted: 29 January 2023
Published: 2 February 2023

1. Introduction

Recently, so-called 'hybrid nanofluids' have attracted the attention of researchers. Hybrid nanofluids are composed of a mixture of two different nanosized particles in a base liquid. The purpose of incorporating hybrid nanoparticles into the base liquid is to enhance the thermal properties of the base liquid by combining the thermophysical properties of the nanomaterials. Due to poor heat transfer in convective liquids such as water and kerosene, nanofluids and hybrid nanofluids have emerged. Due to their high thermal conductivity, hybrid nanofluids have wide applications in engineering, medicine, etc. Choi and Eastman [1] first introduced nanofluids in 1995. They investigated the enhanced heat transfer of nanofluids compared to convective fluids. Crane's study [2] has been key to the study of steady flow across tension sheets. The importance of nanoparticles in improving the thermal capability of water was studied by Prakash and Devi [3]. Nadeem et al. [4] used a hybrid nanofluidic numerical method to study the thermal properties of nanoparticles such as silver and copper. Rashidi et al. [5] used a computational technique to examine the flow of hybrid nanofluids. Nawaz et al. [6] studied the thermal and mass transfer properties of nanofluids along with chemical processes. Shafee et al. [7] analyzed the effect of nanomaterials on heat transfer. Devi et al. [8] studied heat transfer enhancement in hybrid nanofluids. Waini et al. [9] studied the circulation and thermal transfer of hybrid nanofluids through permeable stretchable surfaces.

The flow velocity in the vicinity of an arc is no longer equal to the elongation velocity of the arc. If the cohesive forces are stronger than the adhesive forces, particles near the

surface will not move along with the flow. This is called the slip effect. Joseph et al. [10] studied boundary conditions for permeability walls with sliding movement. Hayat et al. [11] probed the flow of elastic-viscous fluids through stretchable films with partial slip. Bhattacharyya et al. [12] explained the slip effect. Hayat et al. [13] and Sivasankaran et al. [14] studied the slip effect and heat transfer of a nanofluid through a porous area. Salleh et al. [15] analyzed the stability of a boundary layer of a moving fine needle. Xia et al. [16] studied the heat and mass transfer of hybrid nanofluid flows with multiple slip boundary conditions. Wang [17] analyzed gelatinous flow on a stretched sheet with a slip surface. Md. Shoaib et al. [18] carried out a numerical investigation of the MHD flow of a hybrid nanofluid. Adnan et al. [19] studied heat transfer in a nanofluid. Sivanandam et al. [20] analyzed the thermally radiated convective flow of a Jeffery nanofluid. Jagan et al. [21] studied the stratification effect on MHD flow with velocity slip.

Joule heating is a physical effect in which heat energy is generated by passing an electric current through a conductor. Masken et al. [22] investigated heat transfer enhancement in hydrodynamic hybrid nanofluidic flows. Reddy et al. [23] explained the effect of Joule heating on MHD nanofluids. Sajid et al. [24] analyzed the impact of Joule heating on ferrofluids. Daniel et al. [25] reviewed the effect of Joule heating on MHD electrical nanofluids. Kamran et al. [26] carried out a numerical study on magnetohydrodynamic flow in Casson nanofluids along with Joule heating. Khan et al. [27] studied the enhancement of entropy of Williamson nanofluids in the presence of chemical reactions and Joule heating. Gholini et al. [28] carried out an MHD free convection numerical study of Walters B nanofluids on graded stretch films under the influence of Joule heating. Patel et al. [29] analyzed radiation effects on micropolar MHD flow with viscous dissipation and Joule heating. Safwa et al. [30] investigated flow and heat transfer in hybrid nanofluidics with Joule heating.

The estimation of a system's thermal energy (per unit temperature) that is not obtainable for useful work is called entropy. Entropy generation is the amount of entropy during an irreversible process. Heat and mass transfer processes include fluid flow, mixing of substances, expansion of matter, heat exchange, and the motion of bodies. Entropy generation minimization is important for increasing the performance of a system. When there is less irreversibility in the system, much less energy loss occurs. Li et al. [31] studied hybrid nanofluids in nonlinear mixed Marangoni convection with entropy generation. Hussain et al. [32] reviewed entropy analysis in mixed convection in hybrid nanofluids. Kashyap et al. [33] studied the impact of entropy generation in mixed convective hybrid nanofluids. Kasaeipoor et al. [34] studied free convective heat transfer and the cause of entropy in MWCNT MgO/water nanofluids. Ahammed et al. [35] reviewed the entropy production of graphene-alumina hybrid nanofluids. Anuar et al. [36] studied hybrid nanofluidic stagnation point flow in MHDs in the existence of homogeneous-heterogeneous reactions. Rashid et al. [37] performed a theoretical analysis of the MHD flow of hybrid nanofluid with chemical reactions. Krishna et al. [38] studied the radiative MHD flow of He–Casson hybrid nanofluids on porous surfaces. Sivasankaran et al. [39], Arifuzzaman et al. [40] and Kasmani et al. [41] analyzed convection in hybrid nanofluids with chemical reactions. Shoaib et al. [42] studied the entropy generation of the unsteady squeezed flow of MHD carbon nanotubes. Ali et al. [43] analyzed the entropy generation of the Peristaltic flow of nanomaterial in a rotating medium with heat flux. Ramzan et al. [44] carried out an analysis on Entropy generation minimization in the Blasius–Rayleigh–Stokes nanofluid flow through a transitive magnetic field with bioconvective microorganisms.

Homotopy Analytic Method (HAM) is a semi-analytic routine to solve nonlinear ordinary or partial differential equations. The homotopy analysis method uses the homotopy concepts from topology to obtain convergent series solutions of nonlinear systems (see [45–49]). In this paper, we have adapted the Tiwari–Das (see [50]) model. Here, we are studying the flow, temperature, concentration, and entropy production of hybrid nanofluids on porous stretching sheets with convective boundary conditions, slip effects, Joule heating, and chemical reactions.

The present study aims to determine the entropy generation of a hybrid nanofluid flow with convective boundary conditions in the presence of slip effect, Joule heating, and chemical reactions through a porous stretching sheet. Novel to this study, the heat and mass transfer in hybrid nanofluid flow over a porous stretching sheet with convective boundary condition is examined in this study. The study of the heat transfer of convective boundary-layer hybrid nanofluid flows has various applications in mechanical manufacturing processes such as extrusion processes, hydrogen fuel, heat conduction in tissues, electrical-device cooling, mixed hydroelectric dams, large-capacity refrigeration, fuel systems, sunlight, etc.; Investigations of the flow, temperature, concentration and entropy generation with the considered effects are carried out and the results are shown through graphs.

2. Mathematical Formulation

Let us examine a stable two-dimension, incompressible, boundary layer flow of a hybrid nanofluid over a stretching sheet, arranged along the *xy*-plane with the velocity and convective boundary conditions as shown in Figure 1.

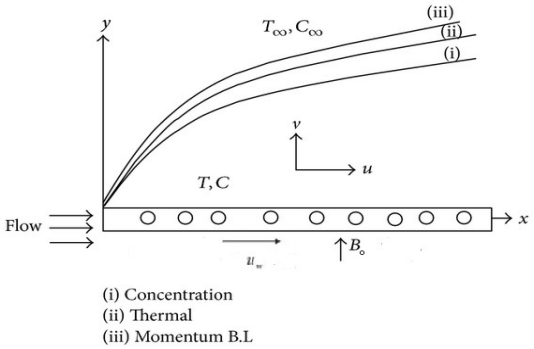

Figure 1. Pictorial description of the problem.

The Continuity, Momentum, Energy, and Concentration equations considering porosity, Joule heating, and chemical reactions are as follows [51–53]:

Continuity Equation

$$\frac{\partial u}{\partial x} + \frac{\partial v}{\partial y} = 0, \tag{1}$$

Momentum Equation

$$u\frac{\partial u}{\partial x} + v\frac{\partial u}{\partial y} = \frac{\mu_{hnf}}{\rho_{hnf}}\left(\frac{\partial^2 u}{\partial y^2} - \frac{u}{k^*}\right) - \frac{\sigma_{hnf}}{\rho_{hnf}}B_o^2 u, \tag{2}$$

Temperature Equation

$$u\frac{\partial T}{\partial x} + v\frac{\partial T}{\partial y} = \frac{k_{hnf}}{(\rho C_p)_{hnf}}\left(\frac{\partial^2 T}{\partial y^2}\right) + \frac{\sigma_{hnf}\, B_o^2}{(\rho C_p)_{hnf}}u^2, \tag{3}$$

Concentration Equation

$$u\frac{\partial C}{\partial x} + v\frac{\partial C}{\partial y} = D_M\left(\frac{\partial^2 C}{\partial y^2}\right) - k_r(C - C_\infty), \tag{4}$$

with boundary conditions [51–53]:

$$\left.\begin{array}{c} \text{at } y = 0: \; u = u_w + u_{slip} = ax + L\frac{\partial u}{\partial y}, v = v_w = 0, \; k_{hnf}\frac{\partial T}{\partial y} = h_s(T - T_w), C = C_w \\ as\; y \to \infty: \; u \to 0, \quad T \to T_\infty, \; C \to C_\infty \end{array}\right\}. \tag{5}$$

where x and y are the cartesian coordinates. The flow occupies the domain $y \geq 0$. The velocity of the sheet along the x-direction is $u_w = ax$, where a is a positive constant. Further, T_w and C_w are the temperature and concentration at the surface, respectively. T_∞ and C_∞ are ambient temperature and concentration, respectively. Here u and v are velocities along x and y axes, respectively. T and C are the temperature and concentration of the hybrid nanofluid, respectively. μ_{hnf}, ρ_{hnf}, k_{hnf}, σ_{hnf}, $(\rho C_p)_{hnf}$ are the viscosity, density, thermal conductivity, electrical conductivity, and heat capacity of the hybrid nanofluid (refer to Tables 1 and 2), respectively. D_M is mass diffusivity, k_r is chemical reaction rate, B_0^2 is magnetic field strength, and k^* is the permeability of a porous medium.

Table 1. Thermophysical properties of Alumina, Copper, and Water (refer to Krishna et al. [38] and El-dawy et al. [53]).

Property	Water	Copper	Alumina
Specific Heat (J/kgK)	4180	385	765
Density (kg/m^3)	997.0	8933	3970
Thermal Conductivity (W/mK)	0.6071	400	40
Electrical Conductivity (s/m)	5.5×10^{-6}	59.6×10^6	35×10^6

Table 2. Thermophysical properties of Nanofluid and Hybrid nanofluid (refer to Krishna et al. [38] and El-dawy et al. [53]).

Thermophysical Property	Nanofluid	Hybrid Nanofluid
Density	$\rho_{nf} = [(1-\phi_1)\rho_f + \phi_1\,\rho_{n1}]$	$\rho_{hnf} = (1-\phi_2)[(1-\phi_1)\rho_f + \phi_1\,\rho_{n1}] + \phi_2\,\rho_{n2}$
Dynamic Viscosity	$\mu_{nf} = \frac{\mu_f}{(1-\phi_1)^{2.5}}$	$\mu_{hnf} = \frac{\mu_f}{(1-\phi_1)^{2.5}(1-\phi_2)^{2.5}}$
Thermal Conductivity	$k_{nf} = \frac{k_{n1}+2k_f-2\phi_1(k_f-k_{n1})}{k_{n1}+2k_f+\phi_1(k_f-k_{n1})}k_f$	$k_{hnf} = \frac{k_{n2}+2k_{nf}-2\phi_2(k_{nf}-k_{n2})}{k_{n2}+2k_{nf}+\phi_2(k_{nf}-k_{n2})}k_{nf}$, where $k_{nf} = \frac{k_{n1}+2k_f-2\phi_1(k_f-k_{n1})}{k_{n1}+2k_f+\phi_1(k_f-k_{n1})}k_f$
Heat Capacity	$(\rho C_p)_{nf} = (1-\phi_1)(\rho C_p)_f + \phi_1(\rho C_p)_{n1}$	$(\rho C)_{hnf} = (1-\phi_2)\left[(1-\phi_1)(\rho C_p)_f + \phi_1(\rho C_p)_{n1}\right]\phi_2(\rho C_p)_{n2}$
Electrical Conductivity	$\sigma_{nf} = \frac{\sigma_{n1}+2\sigma_f-2\phi_1(\sigma_f-\sigma_{n1})}{\sigma_{n1}+2\sigma_f+\phi_1(\sigma_f-\sigma_{n1})}\sigma_f$	$\sigma_{hnf} = \frac{\sigma_{n2}+2\sigma_f-2\phi_2(\sigma_f-\sigma_{n2})}{\sigma_{n2}+2\sigma_f+\phi_2(\sigma_f-\sigma_{n2})}\sigma_{nf}$

Following Devi and Devi [8] and Krishna [38], we are looking for an analogical solution of Equations (1)–(5) by using the suitable variables stated below:

$$\psi = x\sqrt{a\nu_f}f(\eta), \text{where } \psi \text{ is the steam function with } u = \frac{\partial\psi}{\partial y} \text{ and } v = -\frac{\partial\psi}{\partial x}$$
$$\eta = \sqrt{\frac{a}{\nu_f}},\ u = axf'(\eta),\ v = -\sqrt{a\nu_f}f(\eta)\ y, \theta(\eta) = \frac{(T-T_\infty)}{(T_w-T_\infty)}, \phi(\eta) = \frac{(C-C_\infty)}{(C_w-C_\infty)}.$$

We acquire the following ordinary (similarity) differential equations by using the above similarity transformation to Equations (1)–(5):

$$f''' - \frac{f'}{E} + \frac{1}{\mu_{hnf}/\mu_f}\left[\frac{\rho_{hnf}}{\rho_f}\left(ff'' - f'^2\right) - \frac{\sigma_{hnf}}{\sigma_f}Mf'\right] = 0, \tag{6}$$

$$f\theta' + \frac{1}{(\rho C_p)_{hnf}/(\rho C_p)_f}\left(\frac{k_{hnf}}{k_f}\frac{1}{Pr}\theta'' + \frac{\sigma_{hnf}}{\sigma_f}MEcf'^2\right) = 0, \tag{7}$$

$$f\phi' + \frac{1}{Sc}\phi'' - K_r\phi = 0, \tag{8}$$

subjected to:

$$\left.\begin{array}{c} f(0) = 0, f'(0) = 1 + \Lambda f''(0), \theta'(0) = -\frac{k_f}{k_{hnf}}\Omega(1-\theta(0)), \phi(0) = 1 \\ f'(\infty) = 0, \quad \theta(\infty) = 0, \ \phi(\infty) = 0 \end{array}\right\}, \tag{9}$$

where $Pr = \frac{\nu_f}{\alpha_f}$, $M = \frac{\sigma_f B_o^2}{a\rho_f}$, $E_c = \frac{a^2x^2}{(T_w - T_\infty)(C_p)_f}$, $\Omega = \frac{h_s}{k_f}\sqrt{\frac{\nu_f}{a}}$, $Sc = \frac{\nu_f}{D_M}$, $E = \frac{ak^*}{\nu_f}$, $K_r = \frac{k_r}{a}$, $\Lambda = L\sqrt{\frac{a}{\nu_f}}$.

where Pr = Prandtl number, M = Magnetic parameter, E = Porosity parameter, Sc = Schmidt number, Ec = Eckert number, Ω = Biot number, K_r = Chemical reaction parameter, Λ = Slip parameter, and α_f = Thermal diffusivity of a fluid.

The physical parameters such as the skin friction coefficient and local Nusselt number are defined as [8,38]:

$$C_f = \frac{\tau_w}{\rho_f u_w^2}, Nu_x = \frac{xq_w}{k_f(T_f - T_\infty)}, \tag{10}$$

where τ_w is the surface shear stress and q_w is the heat flux from the stretching sheet, which is defined as:

$$\tau_w = \mu_{hnf}\left(\frac{\partial u}{\partial y}\right)_{y=0}, \quad q_w = -k_{hnf}\left(\frac{\partial T}{\partial y}\right)_{y=0}, \tag{11}$$

Using similarity variables solving (10) and (11) we get:

$$Re_x^{\frac{1}{2}}\, C_f = \frac{\mu_{hnf}}{\mu_f} f''(0), \ Re_x^{\frac{1}{2}}\, Nu_x = \frac{k_{hnf}}{k_f}\theta'(0), \tag{12}$$

where Re_x is called the local Reynold's number and it is given by, $Re_x = \frac{u_w x}{\upsilon_f}$.

3. Entropy Generation

The rate of volumetric entropy generation for the current study can be portrayed as (see Li et al. [31], Oztop et al. [54] and Aly et al. [55]):

$$\mathrm{E_G} = \frac{k_{hnf}}{T_\infty^2}\left(\frac{\partial \mathrm{T}}{\partial \mathrm{y}}\right)^2 + \frac{\left(\sigma_{hnf}\, B_o^2\right)}{T_\infty}\,\mathrm{u}^2 + \frac{\mathrm{R}D_M}{T_\infty}\left(\frac{\partial \mathrm{C}}{\partial \mathrm{y}}\frac{\partial \mathrm{T}}{\partial \mathrm{y}}\right) + \frac{\mathrm{R}D_M}{C_\infty}\left(\frac{\partial \mathrm{C}}{\partial \mathrm{y}}\right)^2 + \frac{\mu_{hnf}}{T_\infty k^*}\mathrm{u}^2 + \frac{\mu_{hnf}}{T_\infty}\left(\frac{\partial \mathrm{u}}{\partial \mathrm{y}}\right)^2. \tag{13}$$

Here, the production of entropy is due to heat, mass, fluid friction, Joule heating, and porosity. The characteristic entropy generation is given by [31,54]:

$$E_0 = \frac{k_f(T_w - T_\infty)a}{\upsilon_f T_\infty}.$$

The entropy generation number (N_G) is obtained by dividing volumetric entropy generation and characteristic entropy generation:

$$N_G = \frac{\mathrm{E_G}}{E_0},$$

$$N_G = \frac{k_{hnf}}{k_f}A\theta'^2 + \frac{\sigma_{hnf}}{\sigma_f}MBrf'^2 + B\left[\phi'\,\theta' + \frac{A'}{A}\phi'^2\right] + \frac{\mu_{hnf}}{\mu_f}Br\left[\frac{f'^2}{E} + f''^2\right],$$

where $B = \frac{RD_M(C_w - C_\infty)}{k_f}$, $A = \frac{(T_w - T_\infty)}{T_\infty}$, $A' = \frac{(C_w - C_\infty)}{C_\infty}$, $Br = \frac{\mu_f a^2x^2}{k_f(T_w - T_\infty)}$.

where B = Diffusion Parameter, A = Temperature difference parameter, A' = Concentration difference parameter, and Br = Brinkman number.

The Bejan number is the proportion of heat and mass transfer to the total entropy (see Li et al. [31], Oztop et al. [54] and Aly et al. [55]):

$$Be = \frac{\frac{k_{hnf}}{k_f} A\theta'^2 + B\left[\phi'\,\theta' + \frac{A'}{A}\phi'^2\right]}{\frac{k_{hnf}}{k_f} A\theta'^2 + \frac{\sigma_{hnf}}{\sigma_f} MBrf'^2 + B\left[\phi'\,\theta' + \frac{A'}{A}\phi'^2\right] + \frac{\mu_{hnf}}{\mu_f} Br\left[\frac{f'^2}{E} + f''^2\right]}. \tag{14}$$

Hence, it is clearly seen from (14) that *Be* lies between 0 and 1. When $Be \gg 0.5$, this implies that heat transfer dominates the irreversibility. When $Be \ll 0.5$, the irreversibility is caused because of viscous dissipation, Joule heating, and porosity. When $Be = 0.5$, this implies that the irreversibilities due to heat transfer, porosity, Joule heating, and viscous dissipation are equivalent.

4. Numerical Evaluation Using HAM

The homotopy Analysis Method is used to acquire a solution for the higher number of terms in the approximation series. A higher number of terms improves the accuracy, but the form of the approximation series becomes more expanded. Equations (6)–(8), subject to the initial conditions (9), are solved using the HAM technique. (See [45–49])

Choosing initial guesses as:

$$f_0(\eta) = \frac{1}{1+\Lambda}\left(1 - e^{-\eta}\right),$$
$$\theta_0(\eta) = \frac{\Omega}{\left(\frac{k_{hnf}}{k_f}\right)+\Omega} e^{-\eta},$$
$$\phi_0(\eta) = e^{-\eta},$$

linear operators as $\mathcal{L}_f = f''' - f'$:

$$\mathcal{L}_\theta = \theta'' - \theta,$$
$$\mathcal{L}_\phi = \phi'' - \phi,$$

which satisfies the property:

$$\mathcal{L}_f[C_1 + C_2\exp(\eta) + C_3\exp(-\eta)] = 0,$$
$$\mathcal{L}_\theta[C_4\exp(\eta) + C_5\exp(-\eta)] = 0,$$
$$\mathcal{L}_\phi[C_6\exp(\eta) + C_7\exp(-\eta)] = 0.$$

where C_j (j = 1 to 7) are arbitrary constants.

Using initial guesses and linear operators, the convergence of a solution is found by HAM and appropriate graphs were obtained.

The estimation of the convergence-control parameter (h), which exists in the analytical approximate solution, should be regulated to ensure the convergence of the approximation series [39–43]. This value can be determined using so-called h-curves and tabulated (Table 3). The value of the h_f, h_θ, h_ϕ parameters should be in ranges, $-1.2 < h_f < 0$, $-1.5 < h_\theta < 0.3$ and $-1.4 < h_\phi < 0.2$ (Figure 2). Therefore, when $h = -1$, the convergence of the approximation series is secured and results are acquired.

Table 3. Convergences of series $\phi_1 = 0.01$, $\phi_2 = 0.01$, $\Lambda = 0.2$, $Bi = 0.1$, $Pr = 3.97$, $Ec = 0.3$, $M = 0.5$, $E = 0.3$, $Sc = 0.6$, $K_r = 0.2$.

Order	$-f''(0)$	$-\theta'(0)$	$-\phi'(0)$
1	0.9431	0.0821	0.7028
5	1.0069	0.0773	0.5170
10	1.0089	0.0770	0.4924
15	1.0089	0.0771	0.4873
20	1.0089	0.0771	0.4858
25	1.0089	0.0771	0.4853
30	1.0089	0.0771	0.4851
35	1.0089	0.0771	0.4850
40	1.0089	0.0771	0.4850
45	1.0089	0.0771	0.4850
50	1.0089	0.0771	0.4850

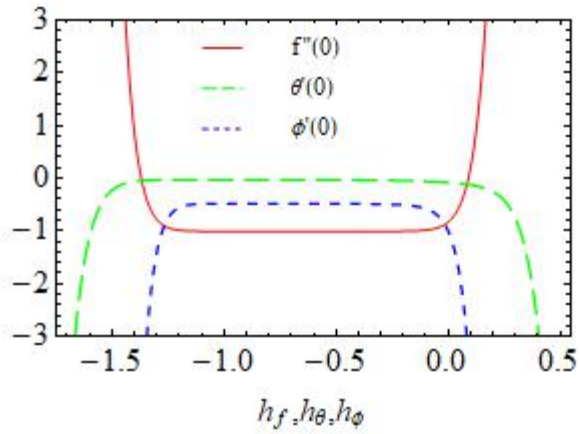

Figure 2. *h*–curve.

5. Results and Discussion

In this current study, we have investigated the effect of involved parameters on velocity, temperature, and concentration. The results are seen through the plotted graphs.

From Figure 3a, we can observe that the velocity profile is decreased as the slip parameter is increased. When the slip parameter increases, the fluid velocity decreases because of the slip condition at the boundary. The dragging of the stretching sheet can only partly be transmitted to the flow of the hybrid nanofluid. In Figure 3b, we can see the dual nature of the solution. At certain values of slip, the temperature first increases and then decreases. In Figure 3c, the concentration increases as the slip parameter increases because there is no friction between the hybrid nanofluid and the surface.

From Figure 4a, we can clearly see that the velocity profile decreases as the porosity parameter increases because, as the permeability of the sheet increases, the hybrid nanofluid will pass through it, which will affect the flow. In Figure 4b,c, it is found that the temperature and concentration increase as porosity increases.

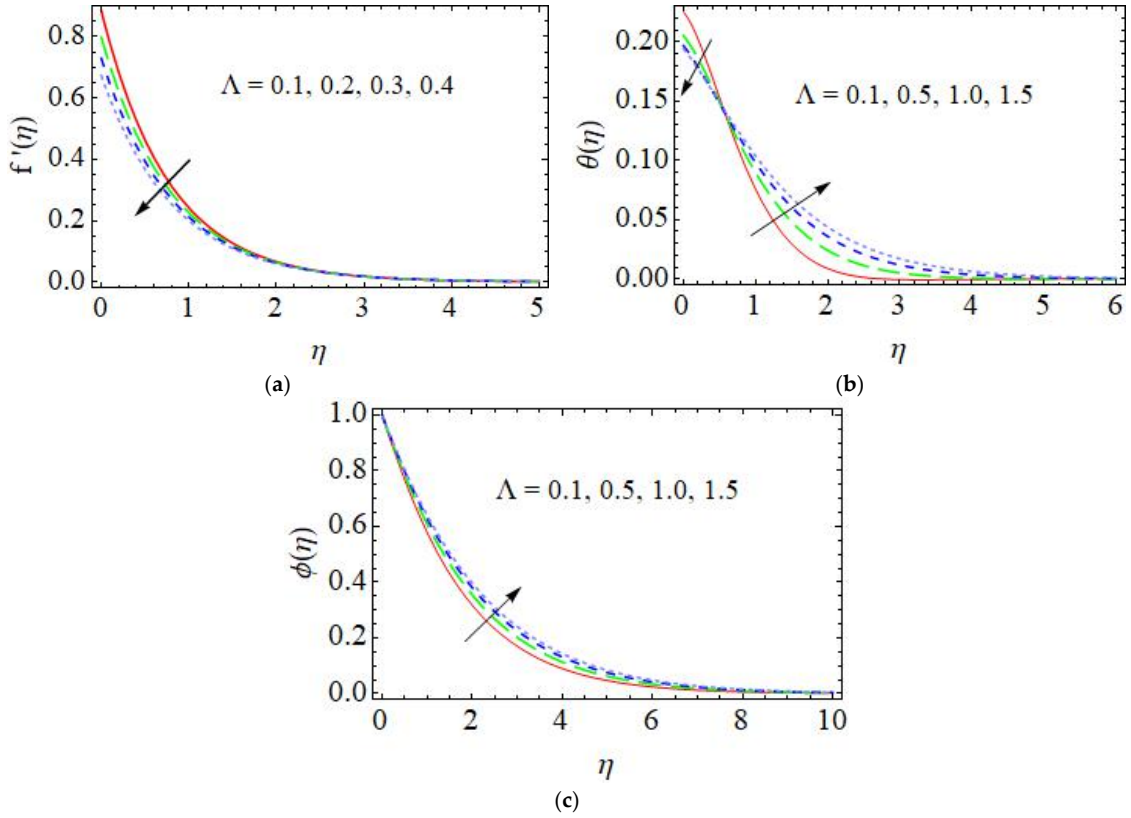

Figure 3. Effect of Slip on (**a**) Velocity, (**b**) Temperature, and (**c**) Concentration profiles.

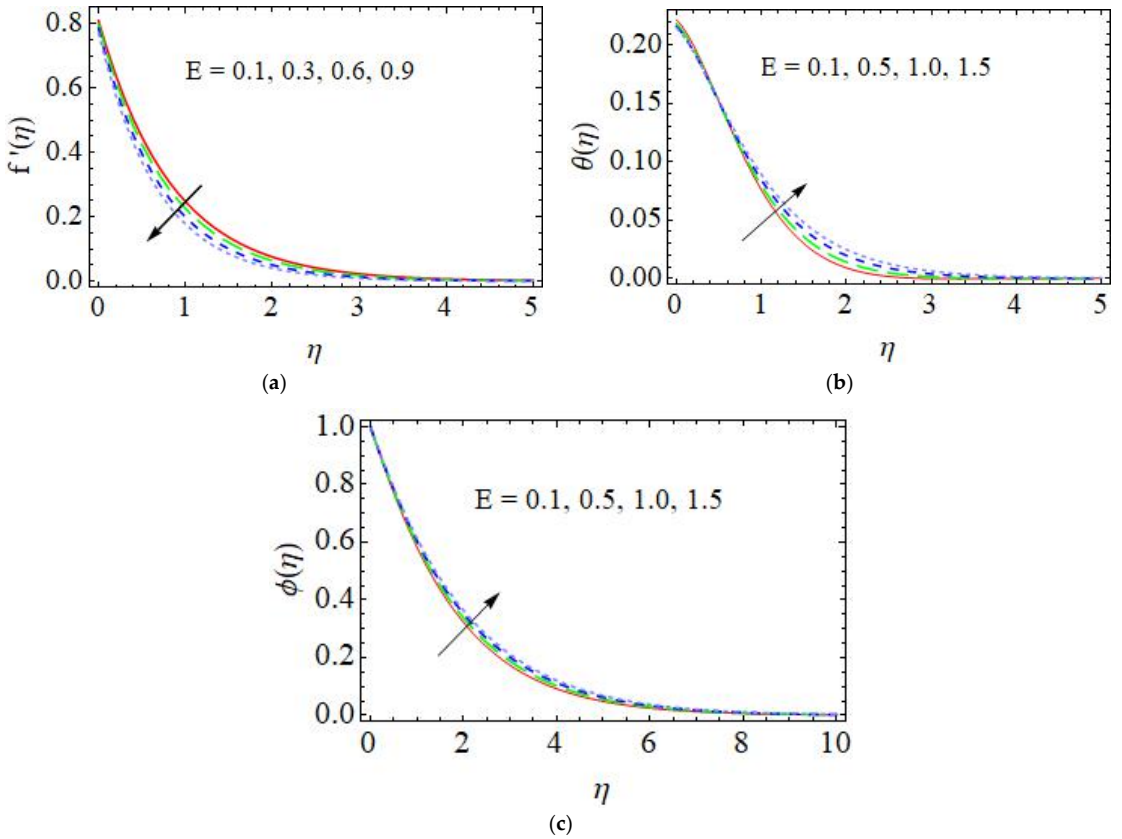

Figure 4. Porosity effect on (**a**) Velocity, (**b**) Temperature, and (**c**) Concentration profiles.

In Figure 5, we can observe that an increase in the Biot number leads to an increase in temperature. Since the Biot number is the function of thermal conductivity, it helps to enhance thermal conduction, thus the temperature increases.

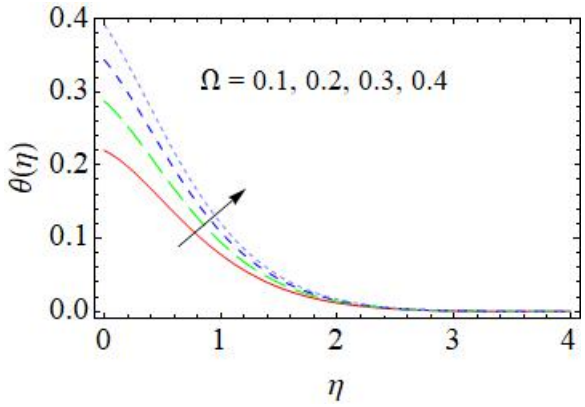

Figure 5. Effect of Biot number on Temperature.

From Figure 6a, we observe that the increment in magnetic parameter leads to a decrease in velocity. This is because the application of a magnetic field to an electrically conducting fluid gives rise to a type of resistive force called the Lorentz force that opposes the fluid flow. However, we observe an increase in the temperature and concentration profiles as the magnetic parameter is increased. This is because the Lorentz force that is produced opposes the fluid flow in the presence of a transverse magnetic field and the resistance provided to the fluid flow is responsible for the increase in the fluid temperature.

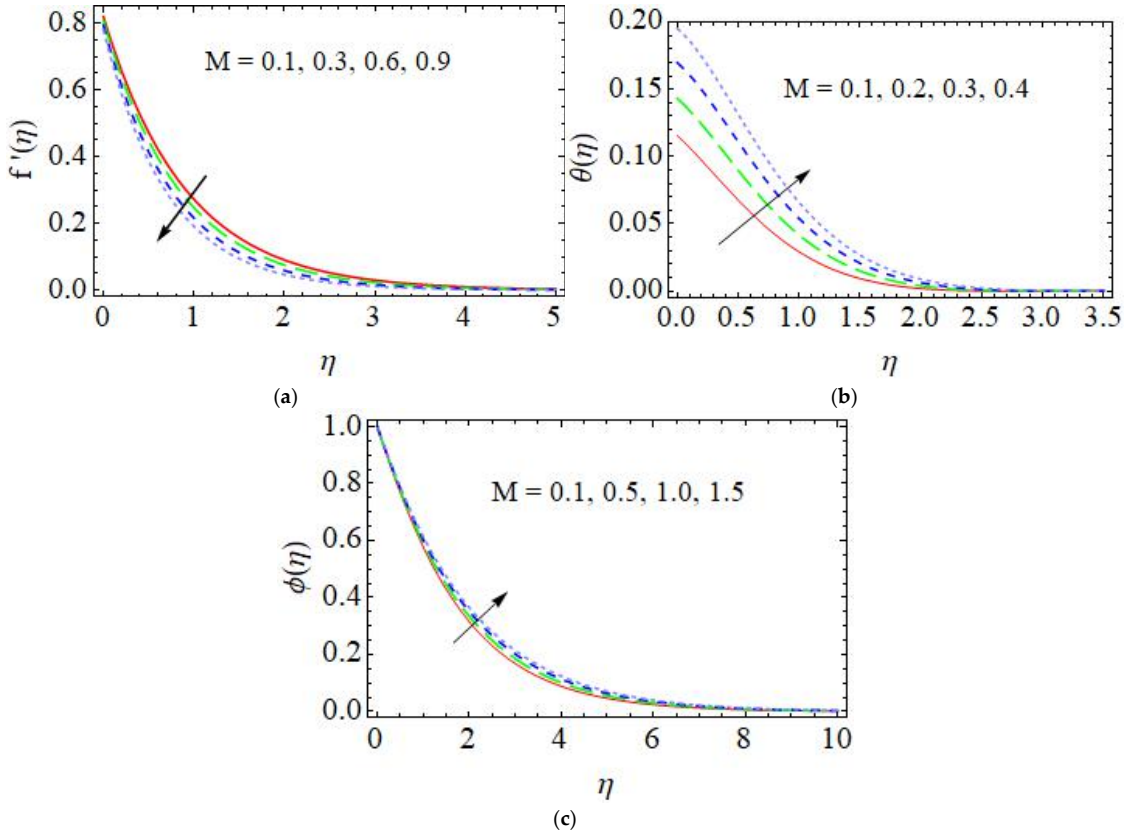

Figure 6. Magnetic effect on (**a**) Velocity, (**b**) Temperature, and (**c**) Concentration profiles.

From Figure 7a,b, a rise in parameter A leads to a decrease in both N_G and Be. Parameter A is associated with temperature difference, according to the definition of entropy, when the temperature difference is high the disorder of the system is decreased, and hence it will reduce the rate of entropy generation. Whereas in Figure 8a,b, a rise in parameter A' increases both N_G and Be. Because A' is the concentration difference parameter, if there is a rise in the concentration difference, then the disorder of the system will increase. This is because, if the concentration is lower in the system, this increases the random motion of the molecules in the hybrid nanofluid. Thus, the rate of entropy generation is high. From Figure 9a,b we can observe that increasing B increases both N_G and Be. We know that B is a diffusion parameter and as, mass diffusivity increases, the density of a hybrid nanofluid will be decreased, which creates a highly disordered system. Hence, the rate of entropy generation is increased. From Figures 10a and 11a, we can see that both the porosity and magnetic parameter show the effect of the dual nature of the solution on N_G. Whereas, Be decreases as both porosity and magnetic parameter increase (Figures 10b and 11b). The higher magnetic field will increase the Lorentz force, which retards the fluid motion, and, thus, in the presence of a strong applied magnetic field, the entropy generation rate decreases.

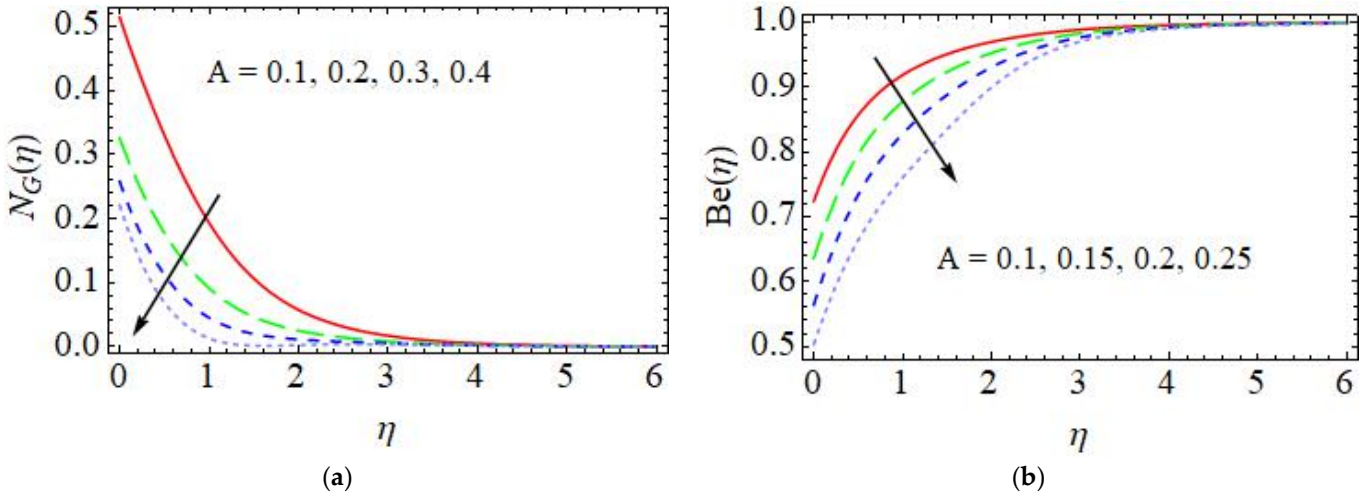

(**a**) (**b**)

Figure 7. Effect of A on (**a**) N_G and (**b**) Be.

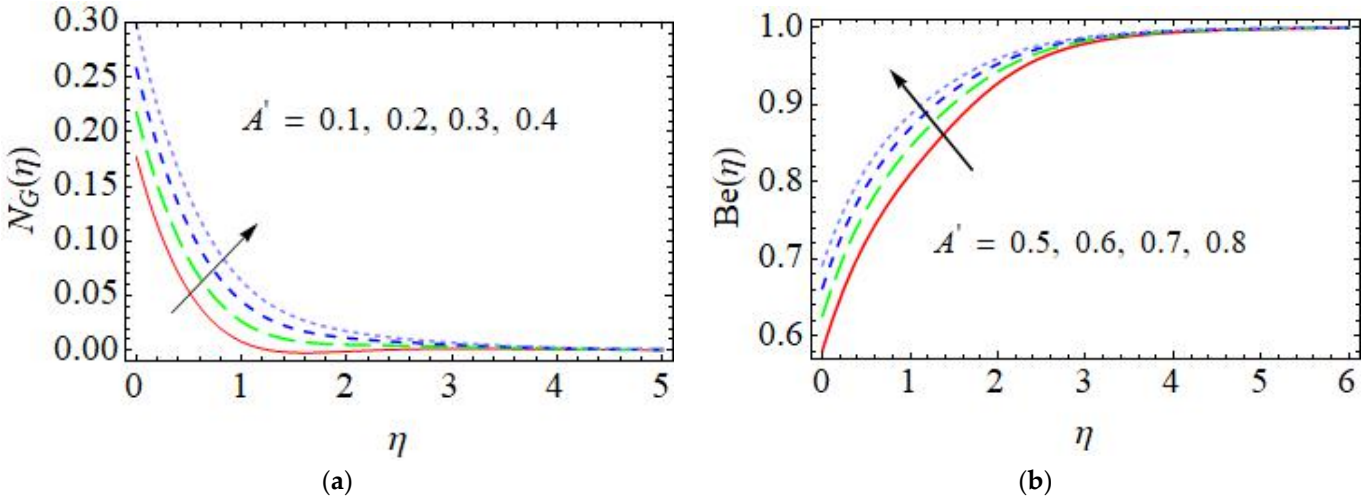

(**a**) (**b**)

Figure 8. Effect of A' on (**a**) N_G and (**b**) Be.

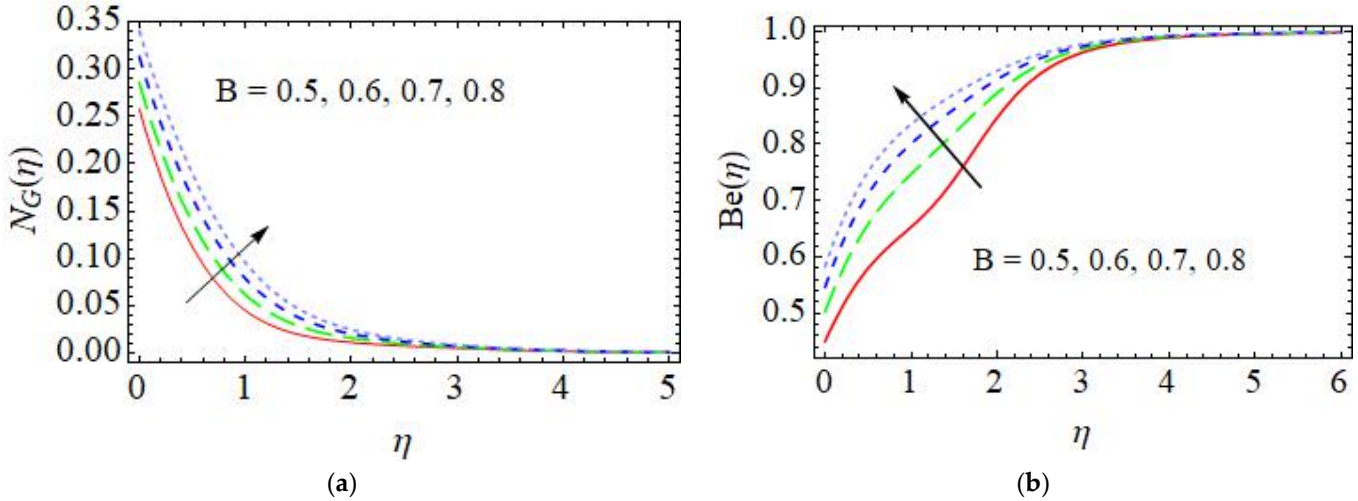

(**a**) (**b**)

Figure 9. Effect of B on (**a**) N_G and (**b**) Be.

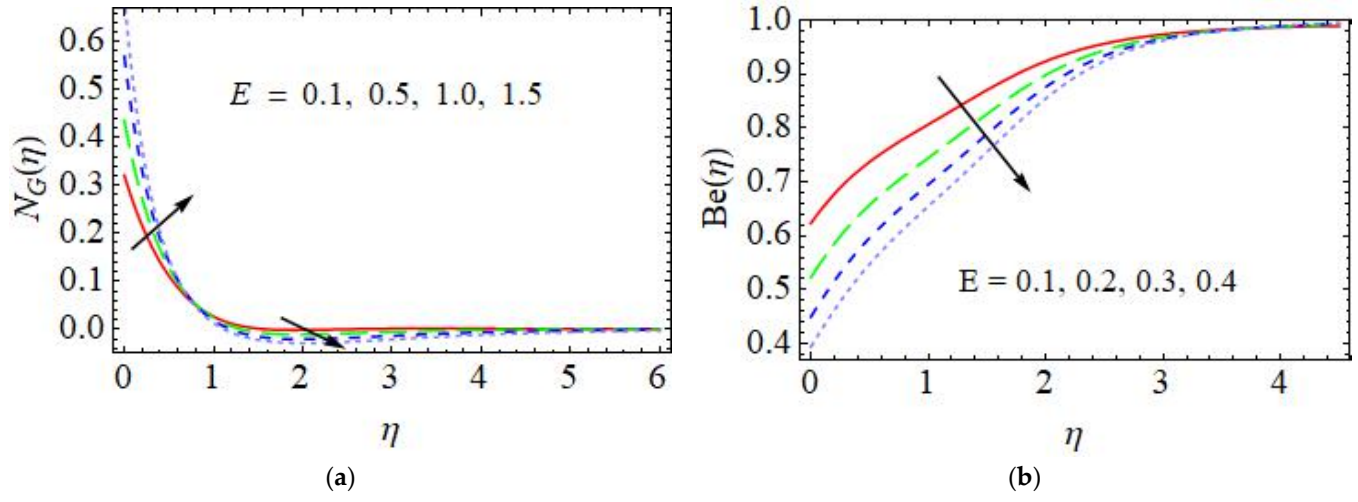

(**a**) (**b**)

Figure 10. Effect of E on (**a**) N_G and (**b**) Be.

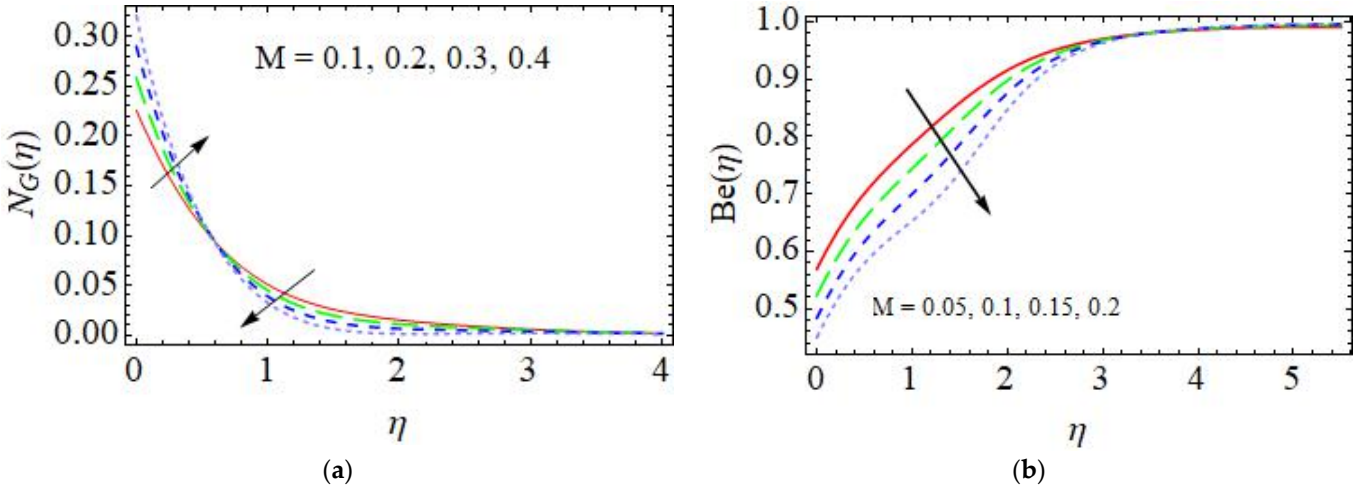

(**a**) (**b**)

Figure 11. Effect of M on (**a**) N_G and (**b**) Be.

From Figure 12, we can detect that, as Br increases, the rate of entropy generation also increases. We know that, physically, *Br* is responsible for the heat transfer via the dual chief sources, i.e., heat generated by viscous dissipation.

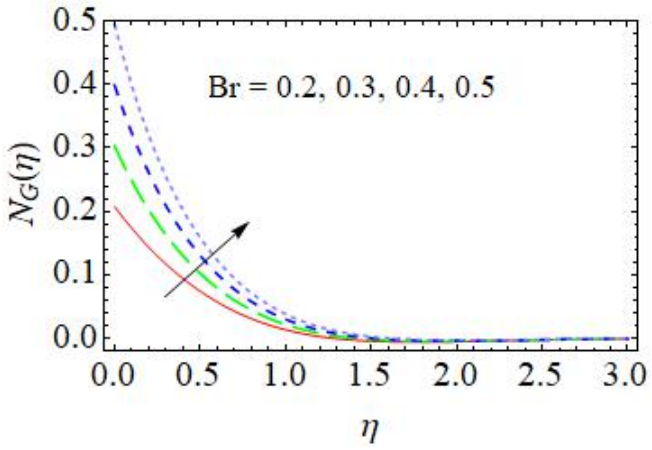

Figure 12. Effect of *Br* on N_G.

6. Conclusions

In this study, the effect of convective, porosity, slip, Joule heating, and chemical reactions on a hybrid nanofluid, and the rate of entropy generation of a hybrid nanofluid over a stretching sheet has been analyzed. The main conclusions are given below.

- An increase in porosity results in a decrease in velocity, whereas, the thermal and concentration profiles are increased. As a result, the rates of both heat and mass transfer increase.
- An increase in the slip parameter decreases the rate of flow of a hybrid nanofluid. The concentration increases as the slip increases.
- An increase in the magnetic parameter increases temperature and concentration but decreases velocity.
- As the Biot number increases, the temperature also increases.
- An increase in the Brinkman number improves the viscous force, which amplifies the collision of fluid particles. Hence, the rate of entropy generation is enhanced.
- When the magnetic parameter is increased there is a decrease in the Bejan number.
- An increase in the Brinkman number increases the rate of entropy generation. Thus, entropy is enhanced due to viscous dissipation.

Author Contributions: Conceptualization, J.K. and S.S.; methodology, J.K.; software, J.K. and M.I.J.; validation, J.K.; formal analysis, J.K., S.S. and M.I.J.; investigation, J.K. and M.I.J.; resources, J.K.; writing—original draft preparation, J.K. and M.I.J.; writing—review and editing, J.K. and S.S.; visualization, J.K.; supervision, J.K. All authors have read and agreed to the published version of the manuscript.

Funding: This research received no external funding.

Conflicts of Interest: The authors declare no conflict of interest.

Nomenclature

u,v	Velocity components taken along x- and y-axes (m/s)
u_w	Velocity at the surface (m/s)
T_w	Surface temperature (K)
C_w	Surface concentration
T_∞	Ambient temperature
C_∞	Ambient concentration

M	Magnetic parameter
E	Porosity parameter
D	Mass diffusivity (m^2s^{-1})
q_r	Heat flux ($kg{\cdot}m^2s^{-3}$)
C_p	Specific heat (J/kg)
T	Temperature of the fluid (K)
C	Concentration of the fluid
k	Thermal conductivity
Pr	Prandtl number
Ec	Eckert number
Sc	Schmidt number
C_f	Skin friction coefficient
Nu	Nusselt number
K_r	Chemical reaction parameter
B	Diffusion parameter
A	Temperature difference parameter
A'	Concentration difference parameter
Br	Brinkman number
Be	Bejan number

Greek symbols

ν_f	Kinematic viscosity of the fluid (m^2/s)
ρ_f	Density of the fluid (kgm^{-3})
μ_f	Dynamic viscosity of the fluid (m^2/s)
α_f	Thermal diffusivity (m^2/s)
σ	Electrical conductivity (s/m)
Ω	Biot number
Λ	Slip parameter

Subscripts

∞	Ambient
f	base fluid
nf	Nanofluid
hnf	hybrid nanofluid

References

1. Choi, S.U.; Eastman, J.A. Enhancing Thermal Conductivity of fluids with nanoparticles. *Mater. Sci.* **1995**, *231*, 99–105.
2. Crane, L.J. Flow past a stretching plate. *Z. Für. Angew. Math. Und. Phys. ZAMP* **1970**, *21*, 645–647. [CrossRef]
3. Prakash, M.; Devi, S. Hydromagnetic hybrid Al_2O_3 -Cu/water nanofluid flow over a slendering stretching sheet with prescribed surface temperature. *Asian J. Res. Soc. Sci. Humanit.* **2016**, *6*, 1921–1936. [CrossRef]
4. Nadeem, S.; Ahmed, Z.; Saleem, S. The effect of variable viscosities on micropolar flow of two nanofluids. *Z. Für. Nat. A* **2016**, *71*, 1121–1129. [CrossRef]
5. Rashidi, M.M.; Raju, C.S.; Sandeep, N.; Saleem, S. A numerical comparative study on 3D nanofluid flows. *J. Comput. Theor. Nanosci.* **2016**, *13*, 4835–4842. [CrossRef]
6. Nawaz, M.; Saleem, S.; Rana, S. Computational study of chemical reactions during heat and mass transfer in a magnetized partially ionized nanofluid. *J. Braz. Soc. Mech. Sci. Eng.* **2019**, *41*, 326. [CrossRef]
7. Sheikholeslami, M.; Zareei, A.; Jafaryar, M.; Shafee, A.; Li, Z.; Smida, A.; Tlili, I. Heat transfer simulation during charging of nanoparticle enhanced PCM within a channel. *Phys. A Stat. Mech. Appl.* **2019**, *525*, 557–565. [CrossRef]
8. Devi, S.U.; Devi, S.A. Heat Transfer Enhancement of Cu–Al_2O_3/Water Hybrid Nanofluid over a Stretching Sheet. *J. Niger. Math. Soc.* **2017**, *36*, 419–433.
9. Waini, I.; Ishak, A.; Pop, I. Hybrid Nanofluid flow and heat transfer past a permeable stretching/shrinking surface with a convective boundary condition. *J. Phys.* **2022**, *1366*, 12022. [CrossRef]
10. Beavers, G.S.; Joseph, D.D. Boundary condition at a naturally permeable wall. *J. Fluid Mech.* **1967**, *30*, 197–207. [CrossRef]
11. Ariel, P.D.; Hayat, T.; Asghar, S. The flow of an elastic-viscous fluid past a stretching sheet with partial slip. *Acta Mech.* **2006**, *187*, 29–35. [CrossRef]
12. Bhattacharyya, K.; Layek, G.C.; Gorla, R.S.R. Slip effect on boundary layer flow on a moving flat plate in a parallel free stream. *Int. J. Fluid Mech. Res.* **2012**, *39*, 438–447. [CrossRef]
13. Hayat, T.; Javed, T.; Abbas, Z. Slip flow and heat transfer of a second-grade fluid past a stretching sheet through a porous space. *Int. J. Heat Mass Transf.* **2008**, *51*, 4528–4534. [CrossRef]

14. Sivasankaran, S.; Mansour, M.A.; Rashad, A.M.; Bhuvaneswari, M. MHD mixed convection of Cu–water nanofluid in a two-sided lid-driven porous cavity with a partial slip. *Numer. Heat Transf. Part A Appl.* **2016**, *70*, 1356–1370. [CrossRef]
15. Salleh SN, A.; Bachok, N.; Arifin, N.M.; Ali, F.M. A Stability Analysis of Solutions on Boundary Layer Flow Past a Moving Thin Needle in a Nanofluid with Slip Effect. *ASM Sci. J.* **2019**, *12*, 60–70.
16. Xia, W.-F.; Ahmad, S.; Khan, M.N.; Ahmad, H.; Rehman, A.; Baili, J.; Gia, T.N. Heat and mass transfer analysis of nonlinear mixed convective hybrid nanofluid flow with multiple slip boundary conditions. *Case Stud. Therm. Eng.* **2022**, *32*, 101893. [CrossRef]
17. Wang, C.Y. Analysis of viscous flow due to a stretching sheet with surface slip. *Nonlinear Anal. Real World Appl.* **2009**, *10*, 375–380. [CrossRef]
18. Shoaib, M.; Raja, M.A.Z.; Sabir, M.T.; Islam, S.; Shah, Z.; Kumam, P.; Alrabaiah, H. Numerical investigation for rotating flow of MHD hybrid nanofluid with thermal radiation over a stretching sheet. *Sci. Rep.* **2020**, *10*, 18533. [CrossRef]
19. Adnan; Khan, U.; Ahmed, N.; Mohyud-Din, S.T.; Alsulami, M.D.; Khan, I. A novel analysis of heat transfer in the nanofluid composed by nanodiamond and silver nanomaterials: Numerical investigation. *Sci. Rep.* **2022**, *12*, 1284. [CrossRef]
20. Jagan, K.; Sivasankaran, S. Three-Dimensional Non-Linearly Thermally Radiated Flow of Jeffrey Nanoliquid towards a Stretchy Surface with Convective Boundary and Cattaneo–Christov Flux. *Math. Comput. Appl.* **2022**, *27*, 98. [CrossRef]
21. Jagan, K.; Sivasankaran, S. Soret & Dufour and Triple Stratification Effect on MHD Flow with Velocity Slip towards a Stretching Cylinder. *Math. Comput. Appl.* **2022**, *27*, 25.
22. Maskeen, M.M.; Zeeshan, A.; Mehmood, O.U.; Hassan, M. Heat transfer enhancement in hydromagnetic alumina–copper/water hybrid nanofluid flow over a stretching cylinder. *J. Therm. Anal Calorim.* **2019**, *138*, 1127–1136. [CrossRef]
23. Reddy, M.G.; Reddy, K.V. Influence of Joule Heating on MHD Peristaltic Flow of a Nanofluid with Compliant Walls. *Procedia Eng.* **2015**, *127*, 1002–1009. [CrossRef]
24. Sajid, M.; Iqbal, S.A.; Naveed, M.; Abbas, Z. Joule heating and magnetohydrodynamic effects on ferrofluid (Fe_3O_4) flow in a semi-porous curved channel. *J. Mol. Liq.* **2016**, *222*, 1115–1120. [CrossRef]
25. Daniel, Y.S.; Aziz, Z.A.; Ismail, Z.; Salah, F. Effects of thermal radiation, viscous and Joule heating on electrical MHD nanofluid with double stratification. *Chin. J. Phys.* **2017**, *55*, 3.
26. Kamran, A.; Hussain, S.; Sagheer, M.; Akmal, N. A numerical study of magnetohydrodynamics flow in Casson nanofluid combined with Joule heating and slip boundary conditions. *Results Phys.* **2017**, *7*, 3037–3048. [CrossRef]
27. Khan, M.I.; Qayyum, S.; Hayat, T.; Khan, M.I.; Alsaedi, A. Entropy optimization in flow of Williamson nanofluid in the presence of chemical reaction and Joule heating. *Int. J. Heat Mass Transf.* **2019**, *133*, 959–967. [CrossRef]
28. Gholinia, M.; Hoseini, M.E.; Gholinia, S. A numerical investigation of free convection MHD flow of Walters-B nanofluid over an inclined stretching sheet under the impact of Joule heating. *Therm. Sci. Eng. Prog.* **2019**, *11*, 272–282. [CrossRef]
29. Patel, H.R.; Singh, R. Thermophoresis, Brownian motion and non-linear thermal radiation effects on mixed convection MHD micropolar fluid flow due to nonlinear stretched sheet in porous medium with viscous dissipation, joule heating and convective boundary condition. *Int. Commun. Heat Mass Transf.* **2019**, *107*, 68–92. [CrossRef]
30. Khashi'Ie, N.S.; Arifin, N.M.; Pop, I.; Wahid, N.S. Flow and heat transfer of hybrid nanofluid over a permeable shrinking cylinder with Joule heating: A comparative analysis. *Alex. Eng. J.* **2020**, *59*, 1787–1798. [CrossRef]
31. Li, Y.X.; Khan, M.I.; Gowda, R.P.; Ali, A.; Farooq, S.; Chu, Y.M.; Khan, S.U. Dynamics of aluminum oxide and copper hybrid nanofluid in nonlinear mixed Marangoni convective flow with Entropy Generation: Applications to Renewable Energy. *Chin. J. Phys.* **2021**, *73*, 275–287. [CrossRef]
32. Hussain, Z.; Alshomrani, A.S.; Muhammad, T.; Anwar, M.S. Entropy analysis in mixed convective flow of hybrid nanofluid subject to melting heat and chemical reactions. *Case Stud. Therm. Eng.* **2022**, *34*, 101972. [CrossRef]
33. Kashyap, D.; Dass, A.K. Effect of boundary conditions on heat transfer and entropy generation during two-phase mixed convection hybrid Al2O3-Cu/water nanofluid flow in a cavity. *Int. J. Mech. Sci.* **2019**, *157*, 45–59. [CrossRef]
34. Kasaeipoor, A.; Malekshah, E.H.; Kolsi, L. Free convection heat transfer and entropy generation analysis of MWCNTMgO (15–85%)/Water nanofluid using Lattice Boltzmann method in cavity with refrigerant solid body-Experimental thermo-physical properties. *Powder Technol.* **2017**, *322*, 9–23. [CrossRef]
35. Ahammed, N.; Asirvatham, L.G.; Wongwises, S. Entropy generation analysis of graphene–alumina hybrid nanofluid in multiport mini channel heat exchanger coupled with thermoelectric cooler. *Int. J. Heat Mass Transf.* **2016**, *103*, 1084–1097. [CrossRef]
36. Anuar, N.S.; Bachok, N.; Pop, I. Cu-Al_2O_3/Water Hybrid Nanofluid Stagnation Point Flow Past MHD Stretching/Shrinking Sheet in Presence of Homogeneous-Heterogeneous and Convective Boundary Conditions. *Mathematics* **2020**, *8*, 1237. [CrossRef]
37. Rashid, A.; Ayaz, M.; Islam, S.; Saeed, A.; Kumam, P.; Suttiarporn, P. Theoretical Analysis of the MHD Flow of a Tangent Hyperbolic Hybrid Nanofluid over a Stretching Sheet with Convective Conditions: A Nonlinear Thermal Radiation Case. *S. Afr. J. Chem. Eng.* **2022**, *42*, 255–269. [CrossRef]
38. Krishna, M.V.; Ahammad, N.A.; Chamkha, A.J. Radiative MHD flow of Casson hybrid nanofluid over an infinite exponentially accelerated vertical porous surface. *Case Stud. Therm. Eng.* **2021**, *27*, 101229. [CrossRef]
39. Sivasankaran, S.; Narrein, K. Numerical investigation of two-phase laminar pulsating nanofluid flow in helical microchannel filled with a porous medium. *Int. Commun. Heat Mass Transf.* **2016**, *75*, 86–91. [CrossRef]
40. Arifuzzaman, M.; Uddin, M.J. Convective of alumina-water nanofluid in a square vessel in presence of the exothermic chemical reaction and hydromagnetic field. *Results Eng.* **2021**, *10*, 100226. [CrossRef]

41. Kasmani, R.M.; Sivasankaran, S.; Bhuvaneswari, M.; Siri, Z. Effect of chemical reaction on convective heat transfer of boundary layer flow in nanofluid over a wedge with heat generation/absorption and suction. *J. Appl. Fluid Mech.* **2015**, *9*, 379–388. [CrossRef]
42. Shoaib, M.; Nisar, K.S.; Raja, M.A.Z.; Tariq, Y.; Tabassum, R.; Rafiq, A. Knacks of neuro-computing to study the unsteady squeezed flow of MHD carbon nanotube with entropy generation. *Int. Commun. Heat Mass Transf.* **2022**, *135*, 106140. [CrossRef]
43. Ali, A.; Sajid, M.; Anjum, H.J.; Awais, M.; Nisar, K.S.; Saleel, C.A. Entropy Generation Analysis of Peristaltic Flow of Nanomaterial in a Rotating Medium through Generalized Complaint Walls of Micro-Channel with Radiation and Heat Flux Effects. *Micromachines* **2022**, *13*, 375. [CrossRef] [PubMed]
44. Ramzan, M.; Gul, H.; Ghazwani HA, S.; Nisar, K.S.; Ahamed Saleel, C. Entropy generation minimization in the Blasius–Rayleigh–Stokes nanofluid flow through a transitive magnetic field with bioconvective microorganisms. *Waves Random Complex Media* **2022**, 1–21. [CrossRef]
45. Liao, S.J. *Beyond Perturbation, Introduction to Homotopy Analysis Method*; Chapman & Hall/CRC Press: Boca Raton, FL, USA, 2003.
46. Liao, S.J. On the homotopy analysis method for nonlinear problems. *Appl. Math. Comput.* **2004**, *147*, 499–513. [CrossRef]
47. Jagan, K.; Sivasankaran, S.; Bhuvaneswari, M.; Rajan, S. Effect of non-linear radiation on 3D unsteady MHD nanoliquid flow over a stretching surface with double stratification. *Appl. Math. Sci. Comput.* **2019**, 109–116. [CrossRef]
48. Jagan, K.; Sivasankaran, S.; Bhuvaneswari, M. Effect of Thermal Radiation on Magneto-Convection of a Micropolar Nanoliquid towards a Non-Linear Stretching Surface with Convective Boundary. *Int. J. Eng. Technol.* **2018**, *7*, 417–421. [CrossRef]
49. Reddy, V.S.; Kandasamy, J.; Sivanandam, S. Impacts of Casson Model on Hybrid Nanofluid Flow over a Moving Thin Needle with Dufour and Soret and Thermal Radiation Effects. *Math. Comput. Appl.* **2023**, *28*, 2. [CrossRef]
50. Tiwari, R.K.; Das, M.K. Heat transfer augmentation in a two-sided lid-driven differentially heated square cavity utilizing nanofluids. *Int. J. Heat Mass Transf.* **2007**, *50*, 2002–2018. [CrossRef]
51. Unyong, B.; Vadivel, R.; Govindaraju, M.; Anbuvithya, R.; Gunasekaran, N. Entropy analysis for ethylene glycol hybrid nanofluid flow with elastic deformation, radiation, non-uniform heat generation/absorption, and inclined Lorentz force effects. *Case Stud. Therm. Eng.* **2022**, *30*, 101639. [CrossRef]
52. Khan, S.A.; Hayat, T.; Alsaedi, A. Thermal conductivity performance for ternary hybrid nanomaterial subject to entropy generation. *Energy Rep.* **2022**, *8*, 9997–10005. [CrossRef]
53. El-dawy, H.A.; El-Amin, M. Effects of Viscous Dissipation and Joule Heating on Micropolar Hybrid Nanofluid in a Stretching/Shrinking Channel including Thermal/Solar Radiation. *Res. Sq.* **2021**. [CrossRef]
54. Oztop, H.F.; Abu-Nada, E. Numerical study of natural convection in partially heated rectangular enclosures filled with nanofluids. *Int. J. Heat Fluid Flow* **2008**, *29*, 1326–1336. [CrossRef]
55. Aly, E.H. Existence of the multiple exact solutions for nanofluids flow over a stretching/shrinking sheet embedded in a porous medium at the presence of magnetic field with electrical conductivity and thermal radiation effects. *Powder Technol.* **2016**, *301*, 760–781. [CrossRef]